# Effective potential of longitudinal interactions between microtubule protofilaments

M. Neek-Amal,[1,*] N. Hamedani Radja,[2,3] and M. R. Ejtehadi[4,†]
[1]*School of Nano, Institute for Studies in Theoretical Physics and Mathematics, P.O. Box 19395-5531, Tehran, Iran*
[2]*School of Physics, Institute for Studies in Theoretical Physics and Mathematics, P.O. Box 19395-5531, Tehran, Iran*
[3]*Instituut-Lorentz, Universiteit Leiden, Postbus 9506, 2300 RA, Leiden, The Netherlands*
[4]*Department of Physics, Sharif University of Technology, P.O. Box 11155-9161, Tehran, Iran*
(Received 12 February 2008; revised manuscript received 24 June 2008; published 21 July 2008)

An effective potential for longitudinal interactions between adjacent protofilaments in a microtubule is introduced. Our proposed interaction potential is a periodic and continuous function of the offset between two protofilaments, which also incorporates the bending energy of protofilaments. This potential produces the results of atomistic simulations. Further, using the potential, a Monte Carlo simulation gives results for the skew angles of observed structures that are in good agreement with experiments.

DOI: 10.1103/PhysRevE.78.011912 PACS number(s): 87.16.Ka, 61.43.Bn

## I. INTRODUCTION

Microtubules (MTs) are ubiquitous in all eukaryotic cells. MTs play key roles in maintaining and protecting the cell structure, and are involved in various cellular processes such as cell division [1]. Studying the MT structures has helped us to better understand their stability, their functions, and their impact on cellular activities [1–4]. Many MT structures have been observed using various experimental methods varying in resolution during the last decades [5–9].

A microtubule is comprised of several protofilaments (PFs) which are arranged on a hollow cylinder with 25 nm in diameter. A protofilament is a polymer of heterodimers, made with the globular polypeptides $\alpha$- and $\beta$-tubulins [10]. MT structures can be characterized by two numbers, $N$ and $s$ indicating the number of constituent PFs, and the number of helices occurring in each turn, respectively. In general, each PF has a longitudinal offset with its immediate neighbors resulting in a net offset $s\delta/2$ for a full turn around the cylinder, where $\delta \approx 8$ nm represents the longitudinal size of heterodimers and $s$ is called helix start number. [11]. Under the assembly conditions, the observed MTs usually consist of either 13 or 14 PFs ($N=13$ or $N=14$) [12,13], where the most common MT structure which is called 13-3 B-lattice structure, consists of 13 nonskewed PFs with a helix start number equal to 3. There is a seam on this structure where $\alpha$- and $\beta$-tubulins are bound laterally [4].

Several findings using different *in vitro* methods such as cryoelectron microscopy, have shown that MTs also assemble with other PF numbers ranging from 10 to 17, and with helix start numbers ranging from 2 to 4 [9]. Moreover, structures with more than one seam are rarely observed [14].

Furthermore, in some of the rare structures, the PFs skew by a small angle around the MT vertical axis [15]. Chrétien *et al.* [4,15] have performed a series of experiments to determine the MT structures. They estimated the PF skew angles with respect to MT axis by measuring the Moiré period, $L_{N-s}$, using a simple geometrical relation [4,15],

$$\sin(\theta_{N-s}) = \frac{\Delta_0}{L_{N-s}}, \tag{1}$$

where $\Delta_0$ is the separation between PFs. Chrétien *et al.* proposed two models for the description of skewed MT structure. Their first model is lattice shear and the second is lattice rotation (see Figs. 4–6 in Ref. [9]). Without having a functional form for the interaction potential, they could not consider the possibility of a combination of lattice shear and rotation [15].

A stochastic model by VanBuren *et al.* [16] has been introduced to investigate the lateral and longitudinal bond energies within the MT lattice. Sept *et al.* [17] investigated the stability of MTs by calculating the binding free energy of adjacent PFs as a function of the longitudinal offsets using an all-atomistic approach. To study the energetics of skewed structures Hunyadi *et al.* considered contributions of three relevant variables, i.e., PF skew angle, MT radius, and longitudinal shear in their expression for free energy [18]. Since the deviations are small, they approximated all the potentials by harmonic functions around their equilibrium. Recently, Hunyadi and Jánosi have investigated the metastability of the MTs by considering the superposition of a simple quadratic bending with either a Lennard-Jones-like or a Morse potential [19].

Here, we show that a minimal information about the structure of the stable microtubules, with considering microscopic symmetries of its building blocks, is sufficient to reasonably model the longitudinal interaction potential between successive protofilaments. The potential has a simple analytical form and mimics the main features of the more detailed potential in Ref. [17] which considers both physics and chemistry of the system. Further, we include a bending energy term in our model in order to quantify the configuration energy of the skewed microtubular structures. We also show that a simple quadratic bending energy has a power-4 form dependence on the skew angle. A Monte Carlo simulation shows that our potential is able to predict the skew angles

*Author to whom correspondence should be addressed; neek@nano.ipm.ac.ir
†Author to whom correspondence should be addressed; ejtehadi@sharif.edu

 

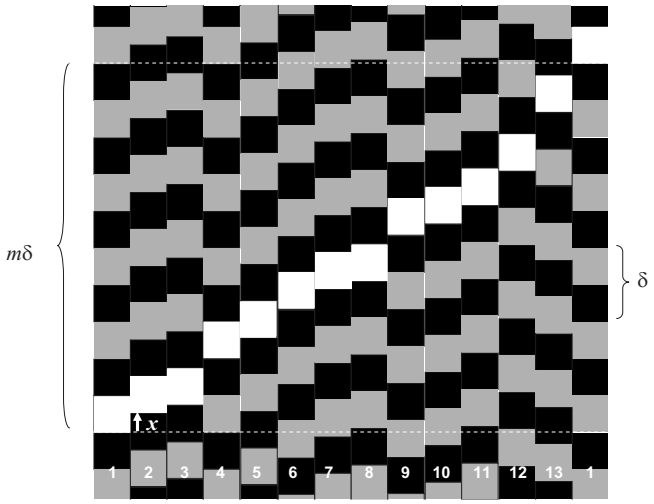


FIG. 1. Flat representation of 13 PFs making a cylinder (as viewed from inside the tube). The arrow indicates the first PF offset. Due to the periodic boundary condition the overall offset is an integer (which is called here the periodicity number) times heterodimer size [Eq. (2)]. Light pathway guides the eyes along a set of positive and bounded $x_i$'s. In this example $m=5$.

and longitudinal offset of protofilaments in good agreement with experimental results [15].

In Secs. II and III we define the general form of our interaction potential for nonskewed and skewed MT structures, respectively. In Sec. IV, a general form for the interaction potential is introduced for 13-3 MT structure, and several tests are presented to reduce the free parameters space. In Sec. V, using annealing Monte Carlo method, we find the skew angles of rare MTs.

## II. MODEL FOR NONSKEWED 13-PF MICROTUBULE STRUCTURE

We consider a set of $N$ (=13) infinitely long filaments of indistinguishable dimers (PF). The longitudinal offset between successive PFs are our model variables, $x_i$ for $i=1,2,\ldots,N$ (Fig. 1). The periodicity in PFs allows us to consider the $x_i$ values to be positive and restricted to the interval $[0,\delta]$. The periodic boundary condition on $x_i$'s and around the tube can be expressed as

$$\sum_{i=1}^{N} x_i = m\delta, \quad m = 0,1,\ldots,N-1, \tag{2}$$

where $m$ is the periodicity number. (In fact $m$ is the helix start number when the dimers are considered as constructing blocks of the tube instead of the monomers.) Due to the identical structure of the PFs, it is highly probable that some $x_i$'s become equal. It is convenient here to partition the set $\{x_i\}$ to $J$ subsets of equal values of $x_i$, each having $n_l$ members and identify a particular MT configuration with $(n_1,n_2,\ldots,n_J)_m$ notation, where $\Sigma_{l=1}^{J} n_l = N$. Therefore, based on the new notation, the 13-3 B-lattice structure is referred to as $(12,1)_2$ B-lattice structure throughout our model.

We now introduce a simple interaction potential between the adjacent PFs as a function of their offsets such that it globally minimizes the energy for the $(12,1)_2$ structure. This is a global minimum condition. Note that the periodic structure of PFs along the MT axis ensures the interaction potential to be a periodic function of the longitudinal offsets. In other words, $u(x)=u(x+p\delta)$ for any integer $p$. Here we ignore the possible changes in the lateral separations between adjacent PFs which are important when MT structure stability and depolymerization are studied [16,19–21]. As a consequence, in our model, the energy of an MT configuration is only a function of offsets

$$E(\{x_i\}) = \sum_{i=1}^{N} u(x_i). \tag{3}$$

To find the ground state, one must find a set of $x_i$'s that globally minimizes the above energy. The minimum energy condition can be obtained by setting the derivatives of $E(\{x_i\})$ with respect to $x_i$'s to be zero

$$\frac{d}{dx_\mu}\left[ E(\{x_i\}) - \lambda\left( \sum_{i=1}^{N} x_i - m\delta \right) \right] = 0, \quad \mu = 1,2,\ldots,N, \tag{4}$$

where $\lambda$ is a Lagrange multiplier containing the periodic boundary condition [Eq. (2)]. Therefore, we have

$$u'(t_1) = u'(t_2) = \cdots = u'(t_N) = \lambda, \tag{5}$$

where the prime symbols refer to derivatives with respect to $x$ and the $t$'s are the $x$ values in minimum energy configuration. Equation (5) is a necessary condition for having local minima, yet, it is not sufficient if one is looking for the global minimum. We expect that the experimentally observed $(12,1)_2$ B-lattice structure, which hereafter is labeled by $(*)$, to be not only a local minimum configuration of MT, but also its stable ground state (global minimum condition). To ensure that $(12,1)_2$ B-lattice structure is indeed the global minimum in our model, we should compare its energy, $E(*)$, with the energy of all other minima, $E(\{t_i\})$. For $(12,1)_2$ B-lattice structure we have

$$t_1 = t_2 = \cdots = t_{12} = t,$$

$$t_{13} = t'. \tag{6}$$

Therefore Eq. (2), Eq. (3), and Eq. (5) for $(12,1)_2$ B-lattice structure are written as

$$12t + t' = 2\delta,$$

$$u'(t) = u'(t'),$$

$$E(*) = 12u(t) + u(t') = 12u(t) + u(-12t). \tag{7}$$

Notice that the periodic condition has been applied when deriving the interaction potential function of the last equation.

The periodic behavior of the interaction potential function enables us to represent the function in the form of the harmonic series

$$u(x) = A_0 + \sum_{n=1} A_n \sin\left[n\left(\frac{2\pi x}{\delta} - \phi_n\right)\right]. \tag{8}$$

The high frequency terms in the Fourier series introduce wiggles to the function that are beyond the resolution of feasible experiments. Therefore, we ignore high frequency terms and try to find the simplest interaction potential, consistent with the experimental results. The interaction potential gives us the global minimum for the most stable $(12,1)_2$ MT experimental structure. Therefore, we start with the lowest frequencies in Eq. (8) to find such an interaction potential.

Taking only the first Fourier term into account, we have

$$u(x) = A_0 + A_1 \sin\left(\frac{2\pi x}{\delta} - \phi_1\right). \tag{9}$$

Without loss of generality we set the first term equal to zero, as it only introduces a constant shift to the energy levels. The $A_1$ coefficient only influences the scaling of the energy; it does not affect the shape of the energy landscape or the minimum energy configuration. Therefore, we can set it to unity and find the interaction potential form in an arbitrary energy unit. To fix $A_1$ we need to incorporate the temperature stability of different structures into our model similar to the work done by Hunyadi *et al.* [18]. Consequently, for the interaction potential in the first harmonic form, only one relevant free parameter, $\phi_1$, is remained to set.

In Sec. IV we will show that this form of the interaction potential cannot describe the global minimum configuration of the $(12,1)_2$ MT structure. Hence, we need to take up to the second harmonic term into account as well, i.e.,

$$u(x) = \sin\left(\frac{2\pi x}{\delta} - \phi_1\right) + c \sin\left[2\left(\frac{2\pi x}{\delta} - \phi_2\right)\right], \tag{10}$$

where $c = \frac{A_2}{A_1}$. This interaction potential has three parameters: $\phi_1$, $\phi_2$, and $c$. Applying the local minimum condition in Eq. (5) for the $(12,1)_2$ B-lattice structure, one parameter can be written in terms of the other two

$$c = \frac{1}{2}\left(\frac{\cos\left(\frac{2\pi t}{\delta} - \phi_1\right) - \cos\left(\frac{2\pi t'}{\delta} - \phi_1\right)}{\cos\left[2\left(\frac{2\pi t'}{\delta} - \phi_2\right)\right] - \cos\left[2\left(\frac{2\pi t}{\delta} - \phi_2\right)\right]}\right). \tag{11}$$

Because of the periodic behavior of the cosine function, our search spaces for both $\phi_1$ and $\phi_2$ are bounded. Note that $\phi_2 \to \phi_2 + \pi/2$ is equivalent to $c \to -c$. Hence, $\phi_2$ is in $[0, \pi/2]$ range while $\phi_1$ can take any value in the range of $[0, 2\pi]$.

To count the possible structures for the 13-PF microtubule configuration according to our model, we can extend the periodicity relation as

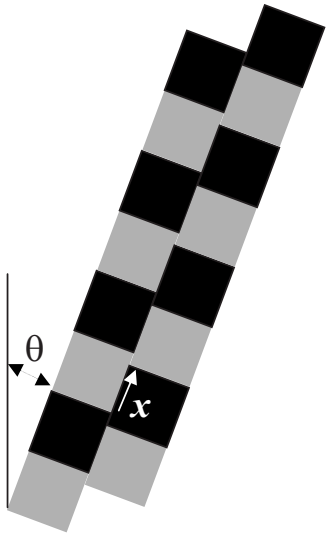


FIG. 2. Two adjacent PFs skewed by an angle $\theta$.

$$n_1 t_1 + n_2 t_2 + \cdots + n_J t_J = m\delta, \quad \sum_{l=1}^{J} n_l = 13, \tag{12}$$

where an occupation number, $n_i$, refers to the number of PFs having an offset equal to $t_i$. In our notation, such MT configuration is labeled by $(n_1, n_2, \ldots, n_J)_m$. Up to the second harmonic term, according to Eq. (5) and Eq. (10), $t_i$'s satisfy

$$\cos\left(\frac{2\pi t_1}{\delta} - \phi_1\right) + 2\cos\left[2\left(\frac{2\pi t_1}{\delta} - \phi_2\right)\right] = \cdots = \cos\left(\frac{2\pi t_J}{\delta} - \phi_1\right) + 2\cos\left[2\left(\frac{2\pi t_J}{\delta} - \phi_2\right)\right] = \lambda. \tag{13}$$

For small values of $\lambda$, these trigonometric equations give rise to at most four real values of $t_i$. Hence, only four possible $n_i$ values are meaningful. For large values of $\lambda$, there exist no real solutions. Therefore considering all possible permutations of $n_i$'s, there are 35 configurations available for 13-PF microtubules. Many of these configurations have not been observed *in vivo* so, and even if one occurs, it must have a greater configuration energy than $(12,1)_2$ B-lattice structure. This fact can be used, in Sec. IV, to confine the search space, for the two remaining parameters ($\phi_1$ and $\phi_2$) in Eq. (10).

## III. MODEL FOR SKEWED MICROTUBULE STRUCTURES

To generalize the above energy model to the skewed MT structures, we consider a set of $N$ very long skewed PFs which bundle to form a closed tube with periodicity number $m$. Therefore, a skewed MT structure can be characterized by the related offsets $\{x_i\}$ and the skew angle $\theta$. Also, we can proceed with positive values of $x$, and either positive or negative values of $\theta$. Two adjacent skewed PFs are illustrated in Fig. 2. In the skewed MT structures, the new periodic boundary condition is written as

$$\sum_{i=1}^{N} x_i + N\Delta_0 \tan(\theta) = m\delta. \tag{14}$$

The skew angle causes a uniform bend in PFs around the tube. As explained in the Appendix, by considering an energy for small bending deformations as a harmonic function of curvature [19,22], one can find the bending potential as a function of skew angle $\theta$ for small angles $[\tan(\theta) \simeq \sin(\theta) \simeq \theta]$. Interestingly, the potential is proportional to the fourth power of $\theta$. Thus,

$$E(\{x_i\}, \theta) = \sum_{i=1}^{N} u(x_i) + \epsilon \frac{\theta^4}{N}. \tag{15}$$

For a skewed MT structure $\epsilon$ is a positive constant parameter which refers to the bending rigidity of an individual PF. $\epsilon$ is an extra parameter to be determined. In contrast to [18] in our model there is no energy potential term for the change in MT diameter, instead we have included the contribution from the curvature. By applying the appropriate periodic boundary condition according to Eq. (14), the minimization leads us to the following equations:

$$u'(t_\mu) - \lambda = 0, \quad \mu = 1, \ldots, N,$$

$$\frac{4\epsilon\theta^3}{N} - \lambda N\Delta_0 = 0. \tag{16}$$

Here $t$'s are the $x$ values in minimum energy configuration for the skewed MT configuration. These equations give rise to an important relationship between the first derivative of $u(x)$ and $\epsilon$,

$$u'(t_\mu) = \frac{4\epsilon\theta^3}{N^2\Delta_0}. \tag{17}$$

The significance of this relationship is that it determines the order of magnitude for $\epsilon$ and enables us to compute its value. Also, since $\epsilon$ should be a positive constant, $\theta$ and $u'(t_\mu)$ must have the same signs. Hence, according to our model, those MTs with negative value of $\theta$ have smaller longitudinal offset with respect to $(12,1)_2$ B-lattice structure, that is, if $\theta < 0$ then $t_\mu < t$ and vice versa. This condition is consistent with the experimental results [15].

## IV. INTERACTION POTENTIAL BASED ON $(12,1)_2$ MICROTUBULE DATA

As mentioned previously, the global minimum of a proposed interaction potential must correspond to the $(12,1)_2$ B-lattice structure. Throughout the paper, we use experimentally reported values ($\delta$=81 Å and $\Delta_0$=51.3 Å) for the length and width of tubulin dimers, respectively. We also consider $t$=9.35 Å for $(12,1)_2$ B-lattice structure [15]. Considering the periodic boundary condition [Eq. (7)], it results in the value $t'$=49.8 Å for the seam offset in the B-lattice structure.

### A. First harmonic term

We start with Eq. (9). Applying the local minimum condition from Eq. (5), $\cos(\frac{2\pi t}{\delta} - \phi_1) = \cos(\frac{2\pi t'}{\delta} - \phi_1)$, fixes the only free parameter of the model, i.e., $\phi_1$. Then,

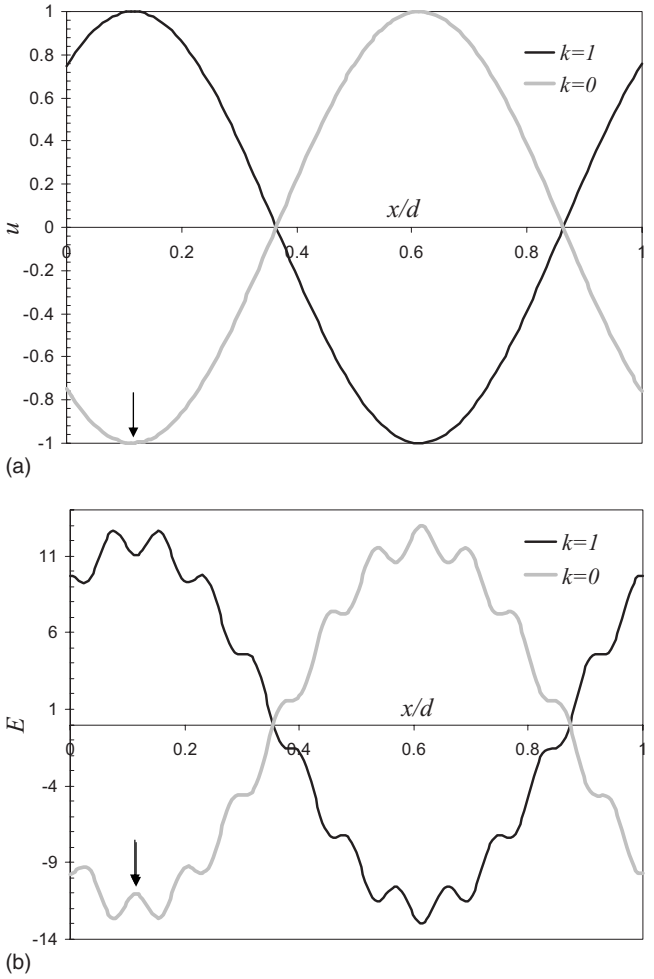


FIG. 3. (a) Longitudinal interaction potential $[u(x)]$ between two adjacent PFs when only the first harmonic term in the Fourier series is taken into account [Eq. (9)]. (b) The corresponding configuration energy of the B-lattice MT $[E(x)]$ using this potential. On the horizontal axes, $x$ is scaled by $\delta$ and energies are plotted in arbitrary units. Arrows in each (a) and (b) correspond to the value of $x$ in the B-lattice structure.

$$\phi_1 = \pi\frac{t + t'}{\delta} + k\pi, \quad k = 0, 1, \tag{18}$$

where $k$ is an integer number. As can be seen from Fig. 3, neither of the $k$ values yield global minimum,

$$E = 12\sin\left(\frac{2\pi x}{\delta} - \phi_1\right) + \sin\left(\frac{2\pi}{\delta}(-12x) - \phi_1\right) \quad \text{at } x = t. \tag{19}$$

Therefore, we need to consider higher order terms in Eq. (8) for constructing the desired interaction potential.

### B. Second harmonic term

Considering terms in Eq. (10) up to the second harmonic term, we have three relevant free parameters: $\phi_1$, and $\phi_2$, and $c$. As a consequence of the local minimum condition, one of

these parameters can be fixed by using Eq. (11). To determine the other two parameters, one can employ the global minimum condition. Consequently, for a successful interaction potential there is no way that other possible 13-PF microtubule structures have configuration energy less than the experimentally observed $(12,1)_2$ B-lattice structure. We utilize this criteria to eliminate the set of $\phi_1$ and $\phi_2$ which do not satisfy the global minimum condition. In the form that we absorbed the free parameters in phases of the sine functions [Eq. (10)], the parameters, $\phi_1$ and $\phi_2$, are bound which allows for the possibility to scan the phase space to find the answer.

### C. Scanning the phase space spanned by two free parameters

According to Eq. (10) and Eq. (11), $\phi_1$ and $\phi_2$ have the periodicity of $2\pi$ and $\frac{\pi}{2}$, respectively. Indeed, a two-dimensional phase space for $\phi_1$ and $\phi_2$ should be searched for reasonable values of the free parameters. Therefore, the area of the original phase space is $2\pi \times \pi/2$. All pairs with the energy less than $E(*)$ have been removed from the list. We have done this practically by performing a simple code that contains the following stages:

(1) All possible values of $\phi_1$ and $\phi_2$ are scanned in two consecutive loops by $\frac{2\pi}{1000}$ and $\frac{\pi}{2\times 1000}$ mesh lengths, respectively.

(2) For each set of $\phi_1$ and $\phi_2$, $E(*)$ is calculated according to the last line in Eq. (7).

(3) In an inner loop the energies of the other 13-PF possible microtubule configurations, $E(\{x_i\})$, have been calculated and compared with $E(*)$. An "if" statement checks the validity of $E(\{x_i\}) < E(*)$ and interrupts the loop if that is true. Otherwise, the loop ends with saving the examined pair of $\phi_1$ and $\phi_2$ as a possible answer.

This algorithm is applied in the following structures respectively.

(i) $(12,1)_m$ *single seam configurations*. The energy of all single seam configurations, $(12,1)_m$ which satisfies periodic boundary condition in Eq. (2) have been checked in the first step. The pair $\phi_1$ and $\phi_2$ have been removed when even one $x$ from the interval $[0,\delta]$ satisfies the condition $12u(x)+u(m\delta-12x) < E(*)$. Running the code results in a small but not vanishing area of acceptable pairs of $\phi_1$ and $\phi_2$ in the region of two-dimensional search space. Here, $\phi_1$ and $\phi_2$ are restricted to $2\pi[0.367,0.615]$ and $\pi/2[0.970,0.985]$ regions, respectively. This is a very tiny region of the original search space which covers only 0.372% of the area of the original space.

(ii) $(13)_m$ *seamless configurations*. A seamless configuration has equal offsets in the successive PFs. It was commonly accepted that MT structures are seamless [23], until the seamed structure was experimentally observed *in vivo* [14]. In the seamless configuration, the periodic boundary condition is written as $13x=m\delta$, where $m$ is an integer in the [0,12] interval. Therefore, only 13 seamless configurations are geometrically possible. For any pair of $\phi_1$ and $\phi_2$, we have checked the global minimum condition, $E(\{x_i\}) > E(*)$, for only 13 different values of $x$. This makes the area of acceptable parameters a little narrower, that is, 0.37% of the original phase space.

(iii) $(n,13-n)_m$ *double-value configurations*. To generalize the seamed configurations which were experimentally observed in Ref. [14], two different values of $x$ have been considered, so that the periodic condition is written as

$$nx_1 + (13-n)x_2 = m\delta, \tag{20}$$

here $n$ is an integer. Obviously, $n=0$ and $n=1$ yield the above two studied configurations. The above equation is also symmetric for $x_1$ and $x_2$. Thus the range of $n$ values reduces to [7,11] range. Considering the global minimum condition,

$$nu(x_1) + (13-n)u(x_2) > E(*), \tag{21}$$

eliminates only a few number of pairs in this step. This makes the area of acceptable parameters 0.369% of the original phase space.

(iv) *Other complex configurations*. By considering the configurations which have three or four numbers of different $x$'s, the procedure of eliminating nonproper pairs can be continued. For three-valued configurations we have examined all pairs of parameters in a similar way. Three-valued configuration is referred to as $(n_1,n_2,13-n_1-n_2)_m$ notation. As we discussed in the preceding section, truncating Fourier series on its second harmonic term guaranteed that a minimum energy configuration never takes more than four different $x$'s. In fact, the most general configuration has $(n_1,n_2,n_3,13-n_1-n_2-n_3)_m$ notation. Looking on the last two structures no pairs of free parameters were eliminated. Therefore, the area of phase space of the meaningful pairs, remains at small portion obtained by considering previous double-valued configurations.

### D. Most significant parameters

The procedure in Sec. IV C demonstrates that a reasonable longitudinal interaction potential between two PFs can be obtained by considering only up to the second harmonic term. Furthermore, we have shown that there are more than one pair of $\phi_1$ and $\phi_2$ that satisfy the global minimum condition. Fortunately, all acceptable pairs of parameters are located in a very tiny region of $\phi_1$-$\phi_2$ space.

It is frequently believed that the $(12,1)_2$ B-lattice structure is the most abundant form of naturally occurring MT [24], while other structures are only rarely found *in vitro*. Accordingly, this structure should be very stable. This allows us to search in an even smaller $\phi_1$ and $\phi_2$ phase space. There are, in fact, two criteria that justify the reduction of parameter search space. First, since there is one seam on the most stable MT structure, we guess that our interaction potential should have two minima, one precisely at $t$ and the other one at around $t'$. We will prove this when we discuss the skewed MT structure results. Second, one way to choose the most significant pair parameters is maximizing the energy gap between the ground state and nearest local minima. Performing the latter criteria, the most significant choice for the parameters become $\phi_1 = 2\pi \times 0.367$ and $\phi_2 = \pi/2 \times 0.980$.

Figure 4(a) exhibits the suggested form of the interaction potential between PFs. The landscape of the total energy, $E(x)$, for single seam structures corresponding to this potential is also shown in this figure. To show $u(x)$ and $E(x)$ in the

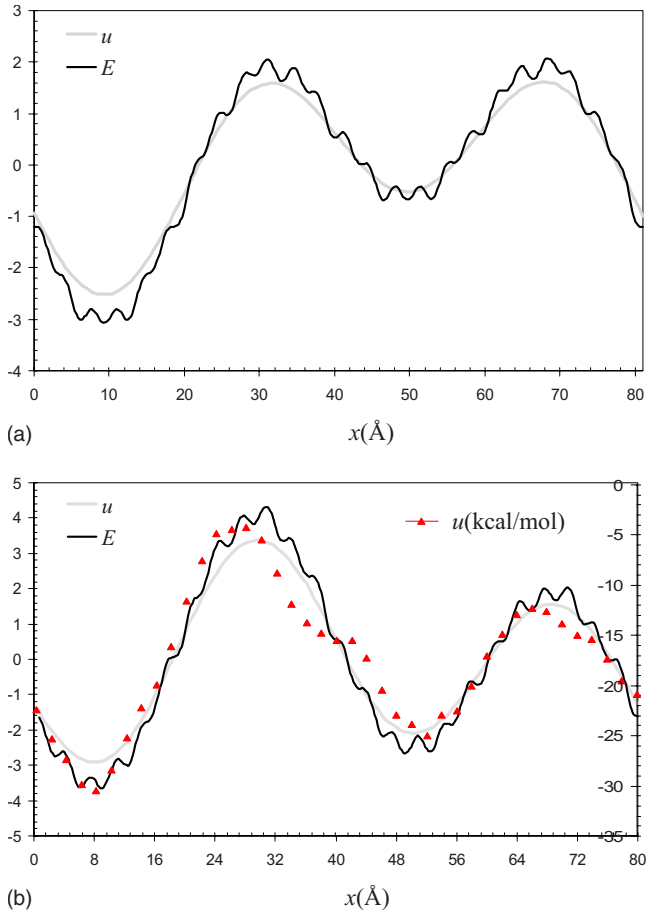


FIG. 4. (Color online) (a) Proposed longitudinal potential $[u(x)]$ between two adjacent PFs (gray) and the corresponding configuration energy $[E(x)]$ for a B-lattice MT (black). (b) The same as above except that the offsets are taken from Ref. [17] which are slightly different offsets from the ones in the B-lattice structure. Picking just this minimal information, the full atomic potential [17,25], red triangles, is obtained. All energies except for the Sept *et al.* potential are shown in arbitrary units.

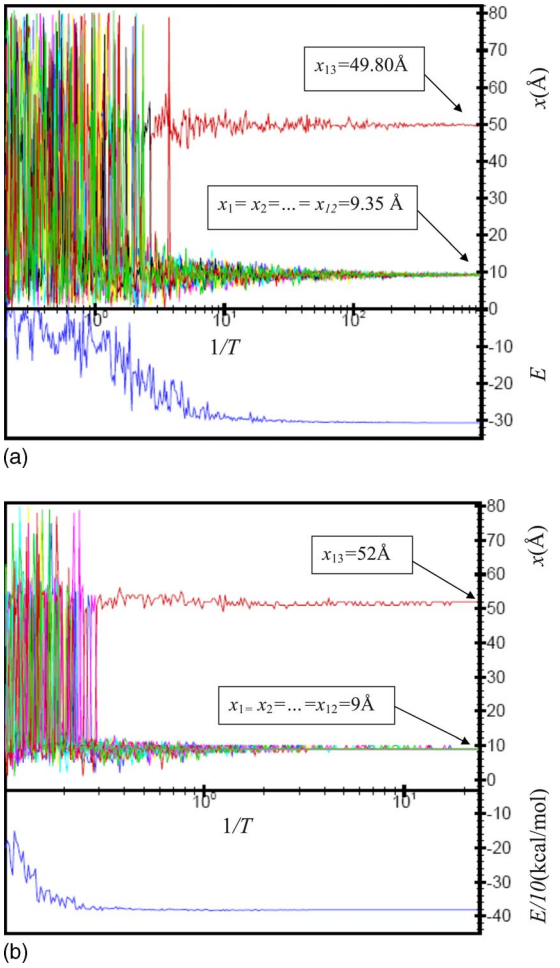


FIG. 5. (Color online) (a) The time trajectory of annealing Monte Carlo simulations for offsets $(x)$ and total energy $(E)$ using proposed interaction potential. As it is expected, a B-lattice structure with 12 regular $x$'s at 9.35 Å and one irregular $x$ at 49.80 Å along the seam is achieved. (b) Same as above, except that the interaction potential in Ref. [17] has been used.

same panel we scaled $E(x)$ by arbitrary energy units. Figure 5(a) depicts an instance of annealing Monte Carlo simulation results with employing $(\phi_1, \phi_2)$ pair. Offsets yield a B-lattice structure with 12 regular $x$'s at 9.35 Å and one irregular $x$ at 49.80 Å along the seam.

Sept *et al.* have recently investigated the lateral and longitudinal interaction potentials between PFs by considering more relevant physical interactions [17]. In this study, they have taken into account both Coulombic and hydrophobic (surface tension) interactions among proteins in the neighboring PFs. Despite some differences, their interaction potential is very similar to the interaction potential obtained here. Triangular symbols in Fig. 4(b) exhibits their results [25]. Furthermore, their interaction potential data points are restricted to the 2 Å resolution that they have used. Their interaction potential does not satisfy the local minimum energy condition [Eq. (5)] for the values of offsets which we have assumed for the $(12,1)_2$ B-lattice structure. The different slopes on the symbolled curve at $t$=9.35 Å and $t'$ =49.80 Å in Fig. 4(b) show this variance.

However, we have employed an annealing Monte Carlo simulation using Sept *et al.* interaction potential. This simulation results showed that the global minimum energy configuration of the interaction potential is a single seamed B-lattice structure with slightly different offset values, i.e., 12 $t_S$=9 Å and one $t'_S$=52 Å [see Fig. 5(b)] which are the same as reported in [17].

To be confident that different values of the offsets are the main source of the difference in the interaction potentials, we repeated all of the above procedures and constructed the interaction potential to find the interaction potential using $t_S$ =9 Å and $t'_S$=52 Å. The results are exhibited in Fig. 4(b). The smooth curve depicts, $u(x)$, and the rough curve corresponds to the total energy. As can be seen from Fig. 4(b), the results are very similar to those obtained in Ref. [17]. It should be noted that neither the energy reference nor the energy scale can be specified within our algorithm. Also, by ignoring higher harmonics in the Fourier series, some details are expected to be lost.

TABLE I. Annealing Monte Carlo simulation results for the PF offsets and skew angles in different microtubular structures. Experimental data and their error bars are taken from Ref. [15]. To compare the notation introduced in the text with the [old] notation of MT structures both are given in the header row.

| $\downarrow x_k$ MT$\rightarrow$ | $(10)_1$ [10-2] | $(11)_1$ [11-2a] | $(12)_1$ [12-2] | $(13)_1$ [13-2] | $(14)_1$ [14-2] | $(11,1)_2$ [12-3] | $(12,1)_2$ [13-3] | $(13,1)_2$ [14-3] | $(14,1)_2$ [15-3] | $(15,1)_2$ [16-3] | $(14)_2$ [14-4] | $(15)_2$ [15-4] | $(16)_2$ [16-4] |
|---|---|---|---|---|---|---|---|---|---|---|---|---|---|
| $x_1$ | 8.647 | 8.347 | 7.986 | 7.704 | 7.501 | 9.320 | 9.350 | 9.314 | 9.079 | 8.870 | 10.074 | 9.591 | 9.220 |
| $x_2$ | 8.770 | 8.357 | 8.033 | 7.704 | 7.467 | 9.363 | 9.349 | 9.290 | 9.078 | 8.845 | 10.090 | 9.554 | 9.263 |
| $x_3$ | 8.739 | 8.394 | 7.998 | 7.728 | 7.479 | 9.305 | 9.348 | 9.310 | 9.105 | 8.843 | 10.035 | 9.587 | 9.188 |
| $x_4$ | 8.722 | 8.349 | 8.018 | 7.732 | 7.429 | 9.333 | 9.350 | 9.294 | 9.087 | 8.860 | 10.094 | 9.591 | 9.227 |
| $x_5$ | 8.794 | 8.335 | 8.026 | 7.701 | 7.419 | 9.359 | 9.349 | 9.314 | 9.090 | 8.860 | 10.114 | 9.573 | 9.253 |
| $x_6$ | 8.766 | 8.377 | 8.039 | 7.696 | 7.444 | 9.324 | 9.350 | 9.286 | 9.094 | 8.853 | 10.118 | 9.580 | 9.188 |
| $x_7$ | 8.686 | 8.358 | 8.022 | 7.704 | 7.494 | 9.333 | 9.351 | 9.296 | 9.087 | **49.271** | 10.096 | 9.548 | 9.202 |
| $x_8$ | 8.741 | 8.373 | 7.997 | 7.707 | 7.421 | 9.346 | 9.352 | 9.284 | 9.078 | 8.875 | 10.106 | 9.593 | 9.241 |
| $x_9$ | 8.735 | 8.388 | 8.030 | 7.732 | 7.492 | 9.316 | 9.350 | 9.296 | 9.075 | 8.857 | 10.051 | 9.584 | 9.203 |
| $x_{10}$ | 8.735 | 8.375 | 8.045 | 7.689 | 7.468 | 9.350 | 9.348 | 9.287 | 9.087 | 8.875 | 10.048 | 9.570 | 9.230 |
| $x_{11}$ | | 8.032 | 8.379 | 7.738 | 7.482 | 9.318 | 9.351 | 9.297 | 9.101 | 8.843 | 10.087 | 9.551 | 9.233 |
| $x_{12}$ | | | 8.024 | 7.724 | 7.435 | **49.757** | 9.351 | 9.299 | 9.101 | 8.856 | 10.130 | 9.552 | 9.232 |
| $x_{13}$ | | | | 7.714 | 7.424 | | **49.801** | 9.2187 | 9.084 | 8.859 | 10.092 | 9.544 | 9.217 |
| $x_{14}$ | | | | | 7.458 | | | **49.717** | 9.080 | 8.851 | 10.094 | 9.554 | 9.220 |
| $x_{15}$ | | | | | | | | | **49.540** | 8.849 | | 9.582 | 9.229 |
| $x_{16}$ | | | | | | | | | | 8.855 | | | 9.222 |
| $\theta_{mc}(^\circ)$ | −1.186 ±0.41 | −1.113 ±0.33 | −1.217 ±0.39 | −1.655 ±0.26 | −1.861 ±0.25 | 0.899 ±0.37 | −0.003 ±0.18 | −0.682 ±0.14 | −1.100 ±0.31 | −1.381 ±0.17 | 1.155 ±0.36 | 1.394 ±0.45 | 1.000 ±0.34 |
| $\theta_{\exp}(^\circ)$ | −1.50 ±0.29 | −2.11 ±0.27 | −1.02 ±0.2 | −1.64 ±0.34 | −2.34 ±0.39 | 0.85 ±0.12 | 0.0 ±0 | −0.68 ±0.12 | −1.33 ±0.16 | −0.51 ±0.05 | 0.87 ±0.13 | 1.81 ±0.23 | 1.17 ±0.15 |

## V. SKEWED MICROTUBULE STRUCTURES RESULTS

So far, since $(12,1)_2$ was a nonskewed MT structure, our calculations were independent of skew angle. Therefore, setting $\theta=0$ in the generalized form of the interaction potential for $(12,1)_2$ structure [Eq. (10)], Eq. (17) yields $u'(t)=u'(t')=0$. As a result there are two minima at $t$ and $t'$ for the interaction potential $u(x)$. This is true for all acceptable values of the remaining phase parameters within the numerical errors.

To estimate the bending rigidity of PFs, $\epsilon$, we need to specify two more variables using experimental data for skewed MT structures. According to the cryoelectron microscopy observations, the $(13,1)_2$ structure is the second most observed structure, the first being the $(12,1)_2$ B-lattice structure. For the $(13,1)_2$ structure $\theta=-0.68^\circ$ and $t=9.27$ Å have been reported [15]. Substituting these values in Eq. (17) yielded $\epsilon=4.373\times10^6$ in an arbitrary energy unit.

*Monte Carlo simulation for skewed microtubule structures*. An annealing Monte Carlo simulation has been employed to find the minimum energy configuration of each MT with $N$ number of PFs. We did the simulation using the interaction potential described in this paper to obtain the skew angle and offsets. We have only run the simulation for those MT structures which have been observed in experiments [15]. We have used the experimental data of $(12,1)_2$ and $(13,1)_2$ MT structures, hence the simulation results should give the correct structures for these two cases.

For each MT configuration, at a given temperature $T$, longitudinal offset of a randomly selected PF have been slightly changing, i.e., $x_k \rightarrow x_k+\zeta$, where $\zeta$ is a random number in the $[-0.05\delta, +0.05\delta]$ range. Then we found the new $\theta$,

$$\theta = \tan^{-1}\frac{m\delta - \sum_{i=1}^{N} x_i}{N\Delta_0},$$

according to Eq. (14). The new values of $x$ and $\theta$ were accepted by the Metropolis rule. In order to expedite trapping the system into its global minimum, an annealing process has been used. To be sure about this trapping, we have repeated the simulation with different initial values.

The results for $t$ and $\theta$ in all investigated structures, and the experimental values for skew angles are reported in Table I. As can be seen from the table all angles are confined between $-2^\circ$ and $2^\circ$. Except for $(11)_1$, $(14)_1$ and $(15,1)_2$ structures, our results are in good agreement with experiment [15]. This could be related to the poor statistics available for these three structures by experiment. Note that, our method produced excellent results for the most observed structures, e.g., $(11,1)_2$, $(14)_2$, and $(12)_1$. The distribution of $\theta$ angles for these structures are shown also in Fig. 6. Overall, when compared to the lattice rotation model (Ref. [15]), our model is more predictive for skew angles (see Fig. 7).

## VI. CONCLUDING REMARKS

We have introduced an effective potential to describe the longitudinal interaction between adjacent protofilaments in

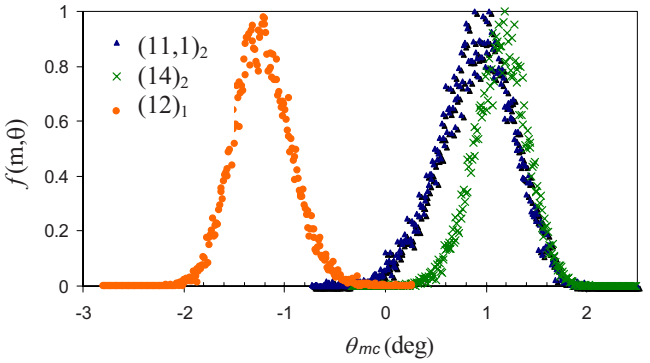


FIG. 6. (Color online) Skew angles distributions, $f(m,\theta)$, for some structures indicated on the legends.

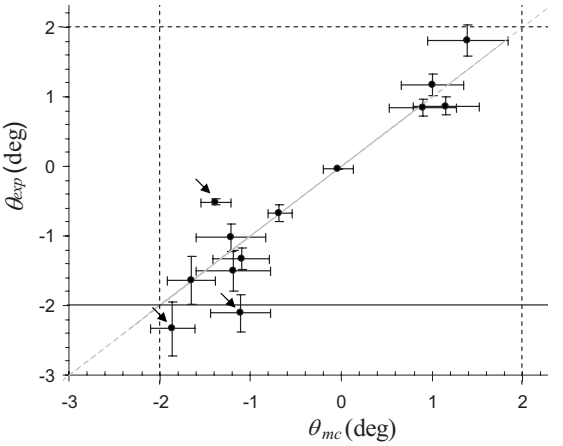


FIG. 7. The interaction potential, proposed in the text, is used to predict the skew angle of protofilaments in different MT structures by using an annealing Monte Carlo simulation. The results (horizontal axis) are compared with the experimental (vertical axis) data. Arrows refer to the results of the least experientially observed configurations. The experimental data and their error bars are taken from Ref. [15].

microtubular structures. The only inputs to our model were the number of protofilaments, the translocation of adjacent protofilaments in the most observed structures $[(12,1)_2]$, the skew angle and translocation of adjacent protofilaments for $(13,1)_2$ microtubule, and finally the width and the height of the tubulin dimers. We have employed annealing Monte Carlo simulation to reproduce microtubule structures with our proposed interaction potential. Moreover, we have generalized the interaction potential by introducing the bending elasticity of the protofilaments by considering the skew angle in $(13,1)_2$ microtubule structure. This new interaction potential permits us to investigate the skew angles which were in good agreement with experimentally observed structures [15]. Although our proposed interaction potential ignores some interactions details and further developments are needed, the consistency between our simulation results and the experiments in this preliminary step is still encouraging.

## ACKNOWLEDGMENTS

We are highly indebted to D. Sept for providing us with the data presented in Fig. 4(b) (symbols). We thank H. Amirkhani for insightful conversations and her valuable comments on the paper. We also thank M. E. Fouladvand and E. Brunk. One of the authors (M.R.E.) thanks the Center of Excellence in Complex Systems and Condensed Matter CSCM for partial support.

## APPENDIX

For an isotropic inextensible rod with length $L$, the bending energy has the form

$$U_B \sim \int_0^L d\ell \left| \frac{d\hat{t}}{d\ell} \right|^2, \tag{A1}$$

where the unit tangent vector $\hat{t}$ indicates the direction of the curve as it winds through space, and $\ell$ is the arc length parameter. In cylindrical coordinates, $(\rho,\phi,z)$, any point on the curve is shown by vector $\vec{r}=\rho\hat{\rho}+z\hat{z}$. Then

$$\hat{t} = \frac{d\vec{r}}{d\ell} = \frac{d\rho}{d\ell}\hat{\rho} + \rho\frac{d\phi}{d\ell}\hat{\phi} + \frac{dz}{d\ell}\hat{z}. \tag{A2}$$

Thus for a helical curve with constant skew angle $\theta$ (angle between $\hat{t}$ and $\hat{z}$) and radius $R$, we have

$$\hat{t} = R\frac{d\phi}{d\ell}\hat{\phi} + \frac{dz}{d\ell}\hat{z} = \sin(\theta)\hat{\phi} + \cos(\theta)\hat{z}. \tag{A3}$$

Considering that $\hat{\phi}$ is the only $\ell$-dependent variable in the above equation, we have

$$\frac{d\hat{t}}{d\ell} = -\sin(\theta)\frac{d\phi}{d\ell}\hat{\rho} = -\frac{\sin^2(\theta)}{R}\hat{\rho}. \tag{A4}$$

The elastic bending energy stored in a helical rod with skew angle $\theta$ and radius $R$ is given by

$$U_B \sim L\frac{\sin^4(\theta)}{R^2}. \tag{A5}$$

Therefore, considering $R=\frac{N\Delta_0}{2\pi\cos(\theta)}$ for small $\theta$ angles the first nonzero term in the PF bending energy is proportional to $\theta^4/N^2$.

[1] J. A. Tuszynski, J. A. Brown, and D. Sept, J. Biol. Phys. **29**, 401 (2003).
[2] Phillip J. Keller, F. Pampaloni, and Ernest H. K. Stelzer, Nat. Methods **4**, 843 (2007).
[3] A. Desai and T. J. Mitchison, Annu. Rev. Cell Dev. Biol. **13**, 83 (1997).
[4] D. Chrétien, S. D. Fuller, and E. Karsenti, J. Cell Biol. **129**, 1311 (1995).
[5] H. Li, D. J. DeRosier, W. V. Nicholson, E. Nogales, and K. H. Downing, Structure (London) **10**, 1317 (2002).
[6] E. M. Mandelkow, E. Mandelkow, and R. Milligan, J. Cell Biol. **114**, 977 (1991).
[7] A. Kis, S. Kasas, B. Babic, A. J. Kulik, W. Benoit, G. A. D. Briggs, C. Schonenberger, S. Catsicas, and L. Forro, Phys. Rev. Lett. **89**, 248101 (2002).
[8] L. Cassimeris, K. Nancy Pryer, and E. D. Salmon, J. Cell Biol. **107**, 2223 (1988).
[9] D. Chrétien and R. H. Wade, Biol. Cell **71**, 161 (1991).
[10] E. Nogales, S. G. Wolf, and K. H. Downing, Nature (London) **391**, 199 (1998).
[11] V. Hunyadi, D. Chrétien, H. Flyvbjerg, and Imre M. Jánosi, Biol. Cell **99**, 117 (2007).
[12] E. M. Mandelkow, R. Schultheiss, R. Rapp, M. Miller, and E. Mandelkow, J. Cell Biol. **102**, 1067 (1986).
[13] G. M. Langford, J. Cell Biol. **87**, 521 (1980).
[14] M. Kikkawa, T. Ishikawa, T. Nakata, T. Wakabayashi, and N. Hirokawa, J. Cell Biol. **127**, 1965 (1994).
[15] D. Chrétien and S. D. Fuller, J. Mol. Biol. **298**, 663 (2000).
[16] V. VanBuren, D. J. Odde, and L. Cassimeris, Proc. Natl. Acad. Sci. U.S.A. **99**, 6035 (2002).
[17] D. Sept, N. A. Baker, and J. A. Mccammon, Protein Sci. **12**, 2257 (2003).
[18] V. Hunyadi, D. Chrétien, and Imre M. Jánosi, J. Mol. Biol. **348**, 927 (2005).
[19] V. Hunyadi and Imre M. Jánosi, Biophys. J. **92**, 3092 (2007).
[20] L. Cassimeris, Cell Motil. Cytoskeleton **26**, 275 (1993).
[21] Imre M. Jánosi, D. Chrétien, and H. Flyvbjerg, Eur. Biophys. J. **27**, 501 (1998).
[22] Imre M. Jánosi, D. Chrétien, and H. Flyvbjerg, Biophys. J. **83**, 1317 (2002).
[23] C. Tanase, Ph.D. thesis, Wageningen Universiteit, 2004.
[24] D. Sept, H. J. Limbach, H. Bolterauer, and J. A Tauzynski, J. Theor. Biol. **197**, 77 (1999).
[25] D. Sept (private communication).